Available online at www.sciencedirect.com
SCIENCE DIRECT®
Journal of Solid State Chemistry 179 (2006) 652–664
JOURNAL OF SOLID STATE CHEMISTRY
www.elsevier.com/locate/jssc

Fe^{3+}-assisted formation of α-Al_2O_3, starting from sol–gel precursors

R. Stößer[a], M. Nofz[b,*], M. Feist[a], G. Scholz[a]

[a]*Institute of Chemistry, Humboldt University, 12489 Berlin, Germany*
[b]*Federal Institute for Materials Research and Testing, 12200 Berlin, Germany*

Received 9 August 2005; received in revised form 16 November 2005; accepted 18 November 2005
Available online 28 December 2005

Abstract

The role of Fe^{3+} ions in the transformations from boehmites and pseudoboehmite xerogels via transition aluminas to corundum was studied here. Especially, the active iron species responsible for the decrease of the temperature of transformation to corundum were looked for. To enable the formation of various Fe^{3+} and Fe^{2+} species, samples were subjected to thermal treatments in different atmospheres as well as mechanically activated. Thermal analysis and ESR spectroscopy served to follow the processes and to characterise the resulting products. It was found that (i) isolated Fe^{3+} ions can indicate local structural changes but have (almost) no influence on the temperature of corundum formation, (ii) the temperature of corundum formation decreases in the result of action of small α-Fe_2O_3 particles and (iii) during thermal treatments Fe^{3+} ions are distributed between different phases or precursors thereof: transition aluminas, corundum, Fe_2O_3, and a Fe^{3+} pool.

Keywords: Redox process; ESR spectroscopy; Thermal analysis; Sol–gel process; Boehmite; Corundum

1. Introduction

Preparation of corundum coatings by application of the sol–gel method at first yields alumina coatings. These have to be transformed to corundum via transition aluminas by thermal treatments. The temperature of thermal treatments for the preparation of corundum coatings on mechanically and thermally stressed metal surfaces has to be kept as low as possible with regard to the unwanted oxidation of the substrates. Thus strategies are asked for to enable the phase transformation to corundum at comparably low temperatures.

The influence of Fe^{3+} ions on the transformation to the α-Al_2O_3 phase, e.g. in the form of ionic admixtures to the respective sol [1,2] or as Fe_2O_3 particles [3,4], is known in its macroscopic aspects. This is a case of "metastable-to-stable" transformation which is not reversible and is not characterised by an equilibrium transformation temperature. Generally speaking, a decrease in the belonging DTA peak temperature T_p with Fe^{3+} concentration c was observed that attained a critical value with $c \approx 0.2$ mol% Fe_2O_3 [2,5].

This threshold leads to the conclusion that competitive processes are at work during the course of thermal transformation of the gels, which will be examined within the scope of this study, among other topics. Furthermore, the phase sequence [6–9] during the above-mentioned transformation, including further macroscopic effects, is also known as a representation of changing macroscopic properties [10–12]. Likewise, numerous research reports have been submitted which relate directly to the material properties (e.g. grain sizes and particle sizes) of Al_2O_3 products, or which concern the use of seeds [2,5,13–15] for T_p reduction.

Because of the findings that have so far been made on the problems implicit in the title and the prevailing assumptions [3,16–19], the present work concentrates on the following problems, which have in the past hardly been dealt with or which have been approached macroscopically and phenomenologically:

(i) Do the Fe^{3+} ions play a key role in changing the thermal properties of the xerogels and in the formation of the Al_2O_3 phases?

*Corresponding author. Bundesanstalt für Materialforschung und -prüfung, Fachgruppe V.4, Richard-Willstätter-Str. 11, 12489 Berlin, Germany. Fax: +49 30 63925976.
E-mail address: marianne.nofz@bam.de (M. Nofz).

0022-4596/$ - see front matter © 2005 Elsevier Inc. All rights reserved.
doi:10.1016/j.jssc.2005.11.026

(ii) Are these species reducible in a chemical manner? Can the oxidation–reduction processes of Fe^{3+} ions, which are initiated by the gas phase, have a direct influence on T_p?
(iii) Within what temperature ranges and how do Fe species take effect (e.g. as Fe^{3+} ions, or in clusters, or in separate phases)?
(iv) Can a significant influence on the transition temperature T_p be achieved by mechanical activation of the matrix or by activation of the two-phase system xerogel/solid Fe compound?

The present work is methodically based on a combination of electron spin resonance (ESR) and thermal analysis (TA). As is well known, ESR provides a selective and sensitive method for characterising paramagnetic species in all states of aggregation [20,21]. In particular, solid systems with centres in ^6S states (such as Fe^{3+} or Mn^{2+} ions) are suitable objects for obtaining local structural information with this method.

XRD and electron diffraction investigations performed on samples treated in the temperature range up to 1300 °C were discussed in [2,5].

The aim of the present TA studies, and particularly the application of the reducing thermal conditions, was to use chemical means to get to know more about the role of Fe^{3+} ions in the above-mentioned phase-transition process to α-Al_2O_3 in association with the ESR method. The TA always provides the indispensable macroscopic evidence for locally acquired ESR results and makes it possible to establish a correspondence between the various descriptive levels, starting from the original, complementary information [22,23].

2. Experimental

2.1. Preparation and transformation of samples

An overview over the samples under study here is given in Table 1.

Commercially available redispersible boehmites Disperal and Disperal P2 (CONDEA Chemie, Germany) and pseudoboehmite samples prepared by hydrolysis of Aluminium(III)-s-butoxide (ASB) in water at 85 °C and partially doped with Fe^{3+} or seeded with corundum (see [2] for details) were included in the studies. The before mentioned samples were subject of thermal treatments at different temperatures and in different atmospheres; details are given in the text and with the figures, respectively.

Some xerogels and mixtures thereof with iron compounds were mechanically activated in a planetary mill (Pulverisette 7, Fritsch, Germany) for different periods of time (8 and 16 h) at 600 rpm. Syalon vials with five syalon balls (12 mm in diameter) were used. The mass of the balls was 14.8 g and that of the samples 1 g.

Table 1
Samples under investigation

Sample	Fe^{3+} content (as mol% Fe_2O_3) or α-Al_2O_3-seeding levels (as mol% Al_2O_3)
	Fe_2O_3 (mol%)
Disperal	$\ll$0.003
Disperal P2	$\ll$0.003
A1	0.003
A2	0.003
A3	$\ll$0.003
Fe004	0.04
Fe013	0.13
Fe026	0.26
Fe052	0.52
Fe104	1.04
	α-Al_2O_3 (mol%)
S100	1.0
S200	2.0

2.2. Thermal analysis

The thermal behaviour was studied mainly by conventional TA (DTA-TG) both in inert and reactive atmospheres. In several cases, simultaneously coupled TA-MS measurements have been applied in order to follow the composition of the evolved gases. A NETZSCH thermoanalyser STA 409 C *Skimmer*®, equipped with a BALZERS QMG 421, was used to record the thermoanalytical curves (T, DTA, TG, DTG) together with the ionic current (IC) curves in the multiple ion detection (MID) mode [24,25]. A DTA-TG sample carrier system with platinum crucibles (baker, 0.8 ml) and Pt/PtRh10 thermocouples was used.

2.3. ESR spectroscopy

ESR spectra in the X-band were taken at room temperature and 77 K with an ERS300 spectrometer (Zentrum für Wissenschaftlichen Gerätebau, Germany). Although for Fe^{3+} ions the g value is close to 2, in the X-band effective g values g' ($g' = h\nu/\beta B$; h is the Planck's constant, ν the microwave frequency, β the Bohr magneton and B the magnetic induction) of up to 20 can result because of the fine structure. Resonance positions were referenced to the signal of a MgO:Cr^{3+} reference sample.

3. Results

3.1. Results of thermal analysis

The key results of the TA are summarised in Fig. 1. It shows the dependence of peak temperature on the concentration of the Fe^{3+} doping of the samples (for the nominally undoped samples the partly very small Fe^{3+} concentrations are estimated by means of the ESR signals). For reasons of comparability, the findings were also

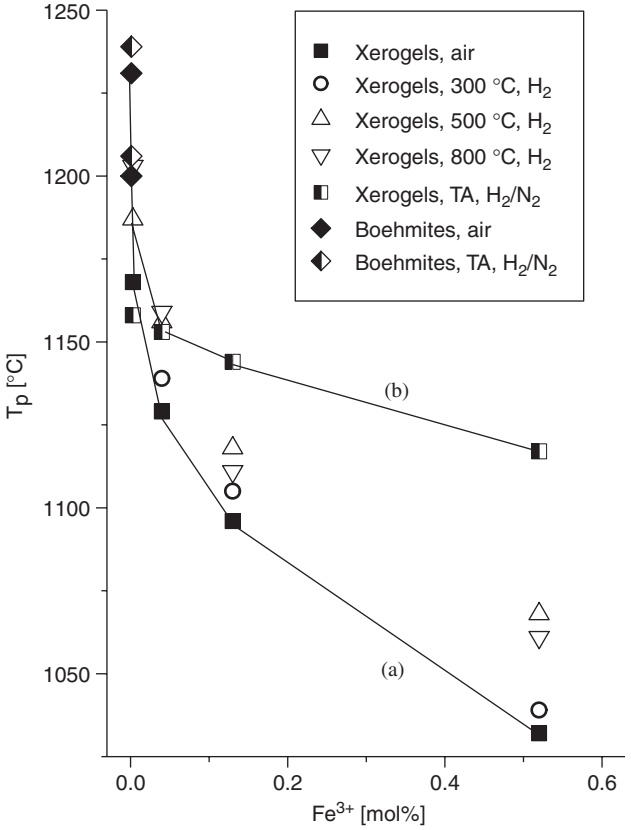

Fig. 1. Influence of Fe^{3+} doping level, chemical, and thermal treatments on the peak temperature of phase transformation to corundum (T_p). Lines (a) and (b) serve as optical guidelines and connect the data points obtained for thermal analysis in a nitrogen or a 10 % H_2/90 % N_2 atmosphere, respectively.

included for selected redispersable boehmites of the disperal type (the data for mechanically treated samples are given in Table 2). Both types of samples avail of only very small Fe^{3+} concentrations.

From the displayed curve progression, it may be directly concluded that the Fe^{3+} ions are the cause of shifts of the peak temperature T_p with higher Fe^{3+} concentrations, not lastly owing to the increasing aggregation of the $\{Fe^{3+}–O\}$ species (see [26–28]). If the TA runs are carried out directly under reducing conditions, remarkable T_p shifts result, accompanied by substantial changes of the respective ESR spectra (see below).

The T_p values resulting from external pre-treatment at 300 °C, 500 °C, and 850 °C in a hydrogen atmosphere are recorded between the two T_p graphs *a* and *b*. Here the combined effect of thermal and chemical influences must be noticed. Moreover, it should also be noted that the sequence of T_p values changes with respect to the pre-treatment temperature with higher Fe^{3+} concentrations. Typical DTA curves were shown in a previous work [2].

Results of TA of samples milled in a planetary mill are summarised in Table 2. It can be seen that mechanical activation enables a decrease of the peak temperature of corundum formation by up to ~140 °C. An additional

Table 2
Samples resulting after mechanical treatments in a planetary mill

Sample	Treatment	Maximum temperature of corundum formation T_p (°C)
A3	None	1148 (air) 1128 (N_2)
A3M08	Milled for 8 h	1049 (N_2)
A3M16	Milled for 16 h	1009 (N_2)
A3Fe_2O_3M	Milled with 1 wt% Fe_2O_3 for 8 h	987 (N_2) 1008 (10 % H_2/90 % N_2)
A3Fe_3O_4M	Milled with 1 wt% Fe_3O_4 for 16 h	1008 (N_2)
A3$Fe(acac)_3$M	Milled with 1 wt% $Fe(acac)_3$ for 8 h	1038 (N_2)

decrease of T_p by milling mixtures of xerogel samples together with iron compounds can only be achieved by addition of Fe_2O_3 whereas Fe_3O_4 or $Fe(acac)_3$ are not as effective.

3.2. Results of the Fe^{3+}-ESR

3.2.1. Basic types of spectral patterns for Fe^{3+} spectra, observed during thermal treatments of xerogels

Fig. 2 is intended on the one hand to give an overview of the diversity of spectral patterns, and on the other hand to show the typically recurring patterns of Fe^{3+}-ESR spectra for the samples, which were recorded before or after the TA. All such spectra can be simulated and can be integrated. But as extensive work on simulation has already been carried out [29], the description and discussion here must be confined to the changes brought about by thermal, chemical and mechanical influences on the samples. These alterations are indicated largely by the effective *g* ratios, g' [20] and the accompanying changes to amplitudes and line widths.

While Fe^{3+} point defects here produce discrete resonances within the range $g'\sim2$, $g'\sim4.3$, and $g'>4.3$ (i.e. $g'\sim5.2$; 13; Fig. 2a), aggregation of the $\{Fe–O_x\}$ species is demonstrated by the overlapping of symmetrical lines of great width in the case of $g'\sim2$ (see Fig. 2b and c). In most cases, these transitions show a distinctive temperature dependence (compare spectra in Fig. 2c and d), since they are brought about by collective magnetic regions, with ferromagnetic or anti-ferromagnetic couplings (see below). These phenomena are accompanied by broadened transitions, particularly at higher Fe^{3+} concentrations. Especially the $g'\sim4.3$ transitions show initial stages of aggregation indicated by their temperature-dependence. This effect is superimposed by magnetic dipole–dipole interactions. The spectrum in Fig. 2b is likewise the result for the Fe^{3+}-doped sample Fe052 after the TA, carried out in a reducing gas atmosphere (10% H_2/90% N_2). Isolated

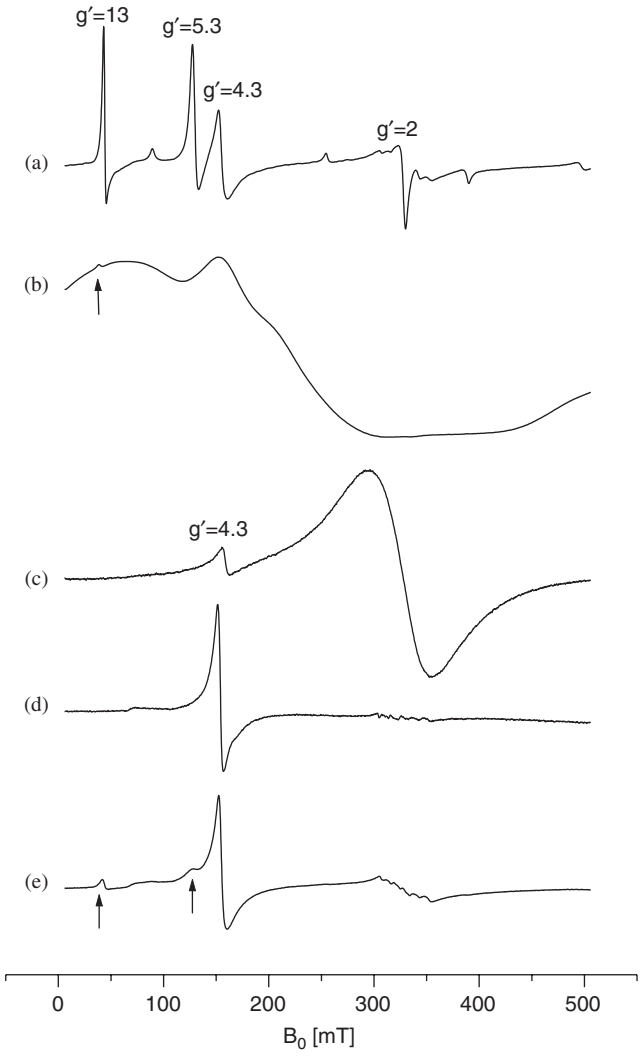

Fig. 2. Typical ESR spectra taken before and after the thermal analysis: (a) sample Fe026, isochronally annealed at 850 °C inside an ESR tube, (b) sample Fe052 after thermal analysis performed in reducing gas (10% H_2/90% N_2), (c, d) sample Fe052, pre-treated for 2 h at 300 K in a hydrogen atmosphere, (e) sample Fe026, isochronally annealed at 750 °C inside an ESR tube and spectrum (d) was taken at 77 K, all others at 293 K.

Fe^{2+} ions are not detectable by ESR under the existing measurement conditions. However, the spectral behaviour (see also [30]) depicted in Fig. 2b arises in interaction of Fe^{2+} with Fe^{3+} ions. Phenomenologically, the formation of finite Fe^{2+} concentrations is made probable by the use of reducing (thermal) conditions and this is last but not least indicated by the pale-green colour of the samples.

Very broad lines with characteristic temperature dependence of intensity, e.g. as depicted in Fig. 2b, unquestionably document the mutual action between Fe^{2+} and Fe^{3+} ions, which summarily leads to a superimposition of ferro- and anti-ferromagnetic contributions. Phenomenologically, there is a sufficient resemblance between the spectrum in accordance with Fig. 2b and that of the mechanically treated ferrimagnetic magnetite. It must also be considered that α-Fe_2O_3 is formed in ferromagnetic or super-paramagnetic form within a range of ~400 °C.

Generally, a simultaneous local formation of α-Al_2O_3:Fe^{3+} seeds (or preliminary stage) is very sensitively shown by the characteristic Fe^{3+}-ESR spectrum (Fig. 2a). The first stages of this process are recognisable in the low field (see arrows in Fig. 2e). The comparatively narrower transitions with g'~13 [31,32] are particularly well suited as sensitive and doubtless indicators for the α-Al_2O_3:Fe^{3+} species and thus for the respective local phase transformation process. Moreover, Fig. 2e depicts the distribution of Fe^{3+} ions between the phases of the matrix formed (i.e. between transition aluminas, corundum and $\{FeO_x\}$), on the basis of the g' values and line widths.

3.2.2. ESR findings before and after thermal analysis, including reductive pre-treatments

In order to gain a further microscopic access to the findings obtained by thermal or chemical means, in addition to the NMR results [5], all of the samples, including selected model substances (see below) were characterised on the basis of their Fe^{3+}-ESR spectra at 293 K as well as 77 K. Typical spectra for Fe^{3+} ions in transition aluminas as well as in α-Al_2O_3 are depicted in Fig. 2d, e and a, respectively. The Fe^{3+} ions are not regularly aligned with O^{2-} ions. OH^- or H_2O molecules are statistically co-ordinated, with a distorted orthorhombic co-ordination polyhedron resulting, giving signals at g'~4.3 [33,34]. Under the chosen conditions, the probability of such an arrangement is relatively high, as it clearly contributes to an approximation of the state of equilibrium of the matrix.

The resonance intensities at g'~4.3 (not shown here) differ only slightly for the Fe^{3+}-doped samples, including the nominally undoped sample A1. Even after drying at 120 °C, part of the Fe^{3+} ions is present in a distorted rhombic co-ordination. With higher degrees of doping (especially with the sample Fe052), a substantial portion of the Fe^{3+} ions is present as an aqueous complex, which is in agreement with the Moessbauer investigations of Huang et al. [16].

The nominally undoped sample A1 contains Fe impurities (<0.01 mol%) which are not only confirmed by the ESR spectrum (see Fig. 3 for the non-zero amplitudes of the g'~4.3 resonances), but also by the pale-brown colour of the sample.

After hydrogen treatment at 300 °C, the spectra of the original xerogels show Fe^{3+} resonances at g'~4.3 with comparatively small line widths. The Mn^{2+} resonances lose intensity as a result of redox reactions (e.g. through the formation of anti-ferromagnetic MnO_2 under the influence of released oxidising components such as NO, NO_2, O_2 [2]). The corresponding integrals of the spectra (not shown here) consequently reveal further findings as a result of the emphasis given to spectral contributions with greater line widths; they provide very broad lines in the region down to B_0~0 mT and, all in all, very broad resonances within the

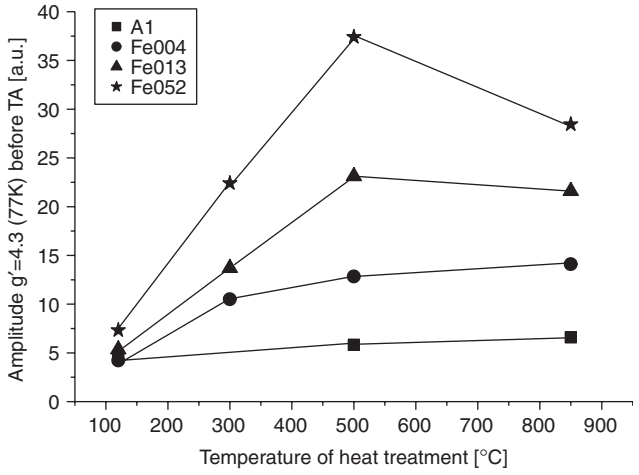

Fig. 3. ESR amplitudes at $g'\sim4.3$ for selected samples as functions of the temperature of pre-treatment in H_2 for 2 h.

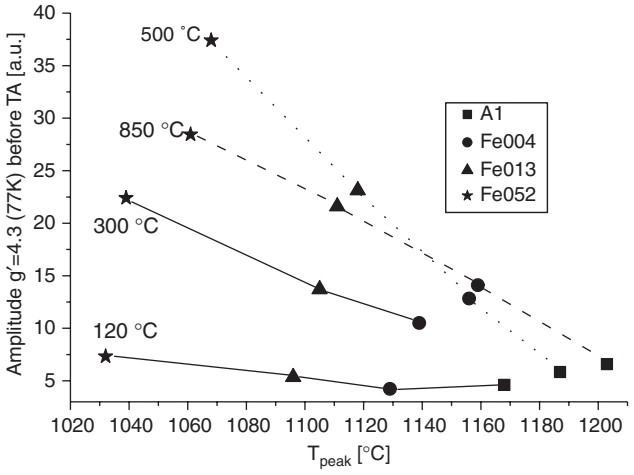

Fig. 4. ESR amplitudes at $g'\sim4.3$ for selected samples in relation to the peak temperatures of corundum formation. The lines connect data points of samples with the same thermal history, i.e. dried at 120 °C or kept for 2 h in a hydrogen atmosphere at 300, 500, and 850 °C, respectively.

$g'\sim2$ range. By comparison with corresponding model systems [35], the latter are allocated to $\{Fe–O_x\}$ aggregates with slight proportions of distorted, i.e. partially paramagnetic MnO_2. In addition, the line width increase is noticeable with growing Fe^{3+} concentration by virtue of the magnetic dipole–dipole interaction at $g'\sim4.3$.

Fig. 3 demonstrates the combined effect of thermal energy and of chemical reduction by hydrogen on the xerogel matrix, on the basis of the amplitudes[1] of the ESR transitions at $g'\sim4.3$. Gel starting samples pre-treated at 120 °C (air) serve as a comparison here. Clearly, the transformation of Fe^{3+} species is dominant within a range of ~300 °C, with very broad lines at $g'\sim2$ into such with $g'\sim4.3$.

At $g'\sim4.3$, the amplitude rises with the increase in the hydrogen pre-treatment temperature (500 °C), particularly with higher Fe^{3+} concentrations (e.g. Fe052). This is due to the complete orthorhombic distortion of the co-ordination sphere by the weakly interactive Fe^{3+} ions, resulting from the release of residual water by the matrix and the local structural reorganisation.

The samples Fe004 and A1 obviously do not have any more reserves regarding available Fe^{3+} ions under these conditions and the amplitudes hardly change with the transition to a temperature of 850 °C. This is all the more surprising, as the reduction power of hydrogen is now clearly increasing. Possibly, no reducible aggregated $\{Fe–O_x\}$ species are left, or this is not accessible within the matrix. A reduction of Fe^{3+} (incorporated in the transition aluminas), based on separate experiments, does not take place or takes place only to a very slight extent. This means, at $g'\sim4.3$ contributions from other species are superimposed on the resonance caused by Fe^{3+} ions in transition aluminas. At $g'\sim4.3$, the amplitudes of the more highly doped samples, Fe013 and Fe052, decrease. This decrease is explained by a reduction of the aggregated $\{Fe–O_x\}$ species during reductive pre-treatment, prior to emplacement of the transitional alumina. This finding presents a further indication for the distribution phenomenon of Fe^{3+} between point defect states and aggregate states of Fe^{3+} ions.

As Fig. 4 makes clear with reference to the amplitudes at $g'\sim4.3$, it must be assumed that there is a connection between reductive pre-treatment of the samples and the observed T_p shift, with xerogels doped with different amounts of Fe^{3+} ions.

It is remarkable that for the doped samples the T_p shifts are comparatively less well pronounced, although the amplitudes clearly increase at $g'\sim4.3$ with the Fe^{3+}-doping level and during treatments in hydrogen at 300 and 500 °C, respectively. However, the Fe^{3+} ions come proportionately from a $\{Fe^{3+}–O_x\}$ pool of xerogels, which contributes largely to the broad transitions at $g'\sim2$ and which feeds the temperature increase as well as the "point defects" with $g'\sim4.3$, as well as the aggregates of type Fe_2O_3. The lowering of the $g'\sim4.3$ amplitude after pre-treatment of the sample with hydrogen at 850 °C makes apparent the reductive power of hydrogen as well as its attack on the aggregate $\{Fe–O_x\}$ prior to the emplacement of Fe^{3+} ions. The formation of Fe^0 species must also be expected under these conditions, especially with hydrogen treatment in the region of 1000 °C. Clearly, the Fe^{3+} concentration represented by the signal with $g'\sim4.3$, is not primarily effective for the formation of corundum. The overall shift of the ascertained T_p values in the direction of higher temperatures indicates that the number of effective Fe_2O_3 seeds was diminished by reduction (see below).

The amplitudes of the ESR signals at $g'\sim2$ and especially at $g'\sim13$ represent a characteristic portion of the Fe^{3+} fine

[1]The first or second integrals of many ESR spectra of the powder samples examined are analysable only after additional corrections. Therefore they are not always more meaningful than the initial deductions which are based on amplitudes and line widths.

structure of α-Al_2O_3:Fe^{3+} (see Fig. 2a). The dependence of the $g'\sim13$ resonance amplitudes on the thermal and chemical pre-treatment as well as their correspondence to the respective T_p values is depicted in Fig. 5. For example, the xerogels which are air dried at 120 °C provide both signal increase (at $g\sim13$) and a decrease of T_p as a function of the Fe^{3+} concentration and thereby confirm the influence of Fe^{3+} ions on the T_p shift—a connection originally derived from macroscopic investigations as mentioned in the introduction.

The $g'\sim2$ region likewise provides a typical signal pattern in the presence of α-Al_2O_3:Fe^{3+} species, which in the case of small Fe^{3+} concentrations is suitable for quantifying the corundum content, and which at higher concentrations indicates the aggregation of the {Fe–O_x} species by signal overlapping.

Surprisingly, reductive pre-treatment of the nominally undoped sample A1 (but which in reality contains traces of Fe^{3+}) provides an increase of T_p, linked with a slight decrease in the ESR amplitudes at $g'\sim2$ and 13, respectively. This trend continues in a slightly modified manner with samples that are rather more highly doped, so that conclusions may be drawn here as well on the original effect of small {Fe–O_x} aggregates (remember also the brown colour of the samples) during phase transformation to α-Al_2O_3.

The reductive effect of hydrogen is particularly noticeable in this series at 500 and 850 °C with the Fe052 sample, which is the most strongly doped with Fe^{3+}. This especially relates to the decrease of the amplitude at $g'\sim13$. The higher doping level also implies the presence of a larger number of reducible {Fe–O_x} aggregates that are no longer available as crystallisation seeds after reduction. At $g'\sim2$, the resulting amplitude is also determined in this case by the distribution of Fe^{3+} ions between the {Al–O} and {Fe–O} phases.

Fig. 6 serves to make apparent a possible connection between the ESR responses of the samples prior to and after performance of the TA; i.e. the amplitudes of the signals at $g'\sim13$ are depicted as a function thereof at $g'\sim4.3$. The picture would be slightly modified with consideration being given to the line widths of the signals. But the basic statement remains unaltered. The integrals of the signals of the respective starting samples exhibit broad signal contributions within the $g'\sim2$ range which must be ascribed to the {Fe−O_x} aggregates and which increase proportionately with the doping concentration.

Although the pre-treatment of the samples at 120 °C (air) only provides a slight differentiation with respect to the amplitudes at $g'\sim4.3$, the signals at $g'\sim13$ increase noticeably after the TA, i.e. proportionally to the Fe^{3+} doping level. With $g'\sim13$, the ESR transition doubtlessly indicates the local corundum formation. The remarkable thing is that pre-treatment of the samples in hydrogen up to temperatures of 500 °C provides a comparatively small increase of amplitudes with $g'\sim13$, although an enlargement of the $g'\sim4.3$ amplitudes was recorded prior to the TA. This means that here, too, competition occurs between the incorporation of Fe^{3+} into the α-Al_2O_3, into the Fe_2O_3 particles, as well as into the transition aluminas. Coupled with redox processes brought about by internal oxidation partners (e.g. decomposition products of nitrate) as well as external (hydrogen) reduction partners, the temperature–time regime adjusts by making a specific distribution of Fe^{3+} ions between the aforementioned phases.

Again at this point it may be concluded that the species with the ESR transitions with $g'\sim4.3$ obviously have only a marginal influence on the α-Al_2O_3 formation in the $T\leqslant850$ °C temperature range. However, they represent Fe^{3+} species which are incorporated in the transitional alumina phases and which are converted by embedding the existing Fe^{3+} species during seed growth into α-Al_2O_3.

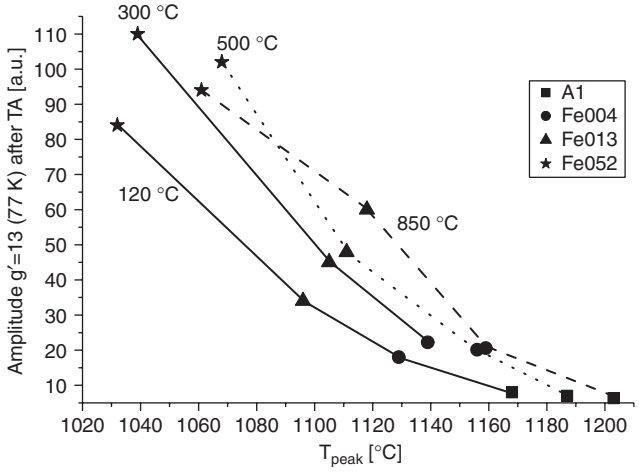

Fig. 5. Amplitudes of the ESR signals at $g'\sim13$ obtained after thermal analysis and the peak temperatures of corundum formation. The lines connect data points of samples with the same thermal history, i.e. dried at 12 °C or kept for 2 h in a hydrogen atmosphere at 300, 500, and 850 °C, respectively.

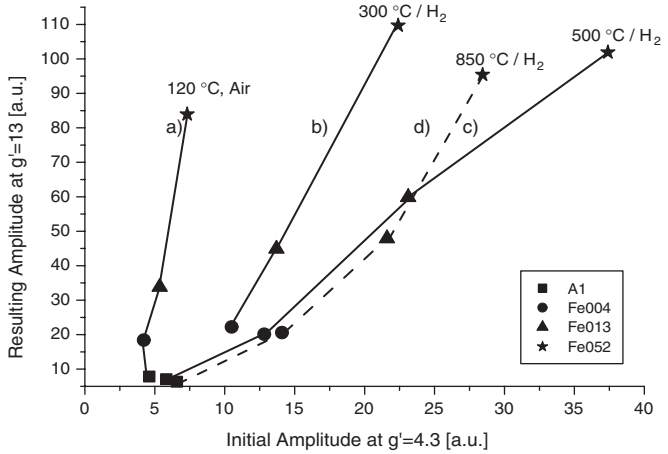

Fig. 6. Relations between ESR amplitudes at $g'\sim13$ obtained after thermal analysis and amplitudes of the ESR signals at $g'\sim4.3$. The lines connect data points of samples with the same thermal history, i.e. dried at 120 °C or kept for 2 h in a hydrogen atmosphere at 300, 500, and 850 °C, respectively.

The shape of the graph in Fig. 6d, which significantly differs from graphs a–c, is obviously determined by the greater reduction power of hydrogen at 850 °C. Part of the potential seeds in the form of small $\{Fe–O_x\}$ aggregates are reducible here and cannot any longer contribute to an increase in the α-Al_2O_3 formation.

All in all, it is interesting to note that the highest amplitudes with $g'\sim13$, respectively, lie within a limited range. This means that these amplitudes are not graded according to the Fe^{3+}-doping concentration of the starting samples. They are rather an expression of the distribution of the Fe^{3+} ions between the {Al–O} and the {Fe–O} phases in formation, whereby the latter have a seeding effect in their early stages and accelerate the formation of corundum.

Fig. 7 provides a further insight into the distribution, seed-formation and seed-growth processes. It can be seen that the temporal development for the ESR amplitudes with $g'\sim13$ (i.e. the representative of α-Al_2O_3:Fe^{3+}) is quite

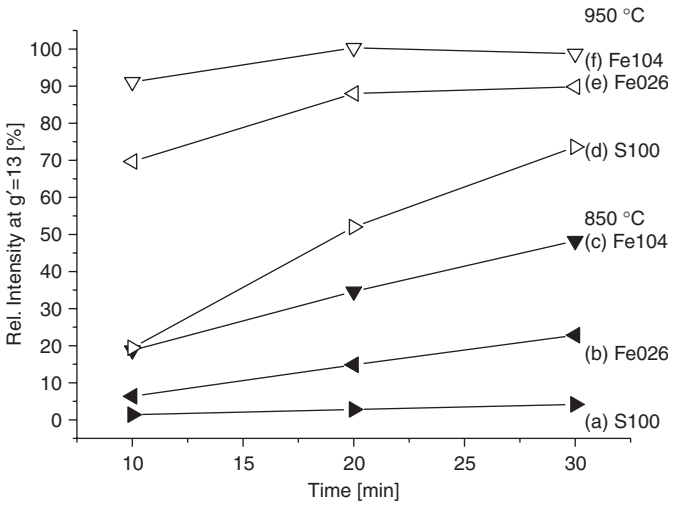

Fig. 7. Time evolution of the amplitudes of the signals at $g'\sim13$ of Fe^{3+} doped and corundum seeded, respectively, xerogels after heat treatments at 850 and 950 °C performed in ESR tubes.

different for systems with corundum seeding or Fe^{3+} doping of the starting sols and provides a further indication of the influence of Fe^{3+} species on the seed-formation process.

In addition, here it should be noted that these samples remained in ESR tubes (3 mm internal diameter, 250 mm in length) during heat treatments in a furnace as well as for the registration of spectra. Because of the tube geometry, this experimental arrangement implies a comparatively high partial water-vapour pressure p_{H_2O} resulting from the water vapourisation and condensation equilibrium in vertically positioned tubes. This high p_{H_2O} (i.e. the saturation vapour pressure at the respective temperature) leads to corundum formation at lower temperatures (e.g. 750 °C) in Fe^{3+}-doped samples and clearly facilitates structural reorganisation. On tempering in a quartz insert (internal diameter 20 mm, height 250 mm) in the furnace, the partial water-vapour pressure that sets in is noticeably lower and the formation of corundum takes place only at higher temperatures even with the same samples.

While the seeded sample (S100) showed hardly any changes in what was a small amplitude anyway with $g'\sim13$ (Fe^{3+} impurities of the xerogels), after treatment at 850 °C in each case, a clear increase was registered by the sample doped with Fe^{3+}. Here, seed formation has to dominate, followed by a finite seed growth. For the seeded sample, this seems to be relevant only at 950 °C—combined with the embedding of Fe^{3+} in the α-Al_2O_3 matrix. The Fe^{3+}-doped samples here attain a somewhat stationary state, as the number of effective seeds does not continue to grow markedly and seed growth becomes decisive.

3.2.3. Distribution of Fe^{3+} between transition aluminas, α-Al_2O_3 and $\{Fe–O_x\}$ phases

As Fig. 8a shows, a finite concentration of species with $g'\sim4.3$ is present at crystallisation temperatures (T_p). And while the amplitudes with $g'\sim4.3$ dominate in the case of the undoped or little doped samples, a stationary value results for the quotients above about 0.2 mol% Fe^{3+}. This

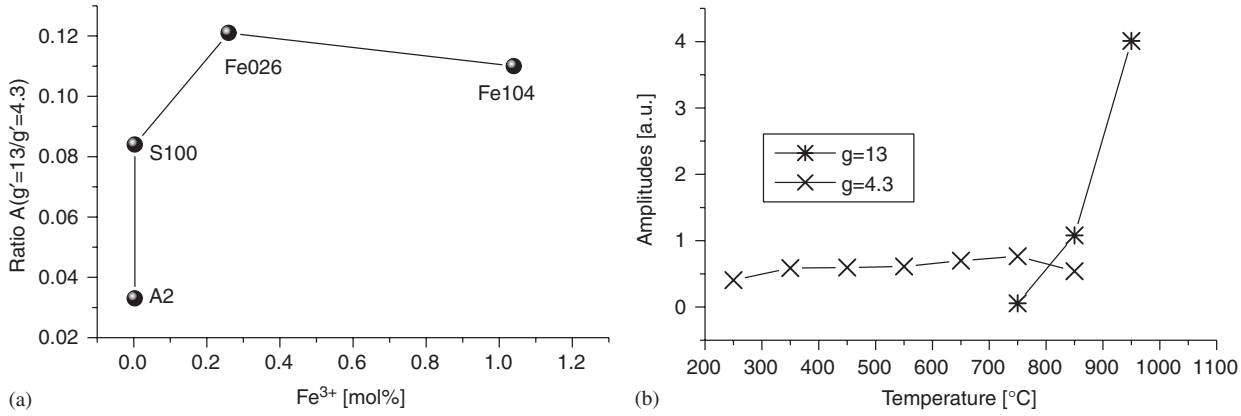

Fig. 8. (a) Ratio of ESR amplitudes at $g'\sim13$ and 4.3 graphically represented as functions of the corresponding Fe^{3+} concentrations. The amplitudes were obtained for different xerogels (nominally undoped, corundum seeded and Fe^{3+} doped) heated in the thermobalance until the respective temperatures of most intense lattice formation. (b) Amplitudes of ESR transitions at $g'\sim4.3$ and $g'\sim13$ of sample Fe026 as a function of the temperature of heat treatments in air (30 min at each temperature).

means that the number of Fe^{3+} ions embedded in the corundum rises until it reaches a limiting value. It is only with a further rise in temperature (or lengthening of the tempering time) that the remainder of the species is converted, with $g'\sim4.3$, and the Fe^{3+} is embedded in the corundum. So it is then that several species (α-Al_2O_3, transition aluminas and related phases) as well as residues of $\{Fe–O_x\}$, which are not suitable for seeding, co-exist under the experimental thermoanalytical conditions.

In accordance with Fig. 8b, amplitudes within the range $g'\sim4.3$ show only a slight dependence on the pre-treatment temperature (sample Fe026) up to about 750 °C. Only when it is above this temperature does the amplitude of the broad lines at $g'\sim4.3$ drop. This amplitude change is less pronounced as a result of the greater line width relating to signals with $g'\sim13$ (α-Al_2O_3:Fe^{3+}).

Accordingly, a steeper slope emerges for signal amplitudes with $g'\sim13$. With $g'\sim13$, the narrow line width is the result of the less well-pronounced angular dependence of the signals, or their low dependence on the statistic distribution of zero field parameters [24].

In Fig. 9, the signal amplitude quotients are used, with $g'\sim13$ and 4.3, on the one hand in order to reduce experimental amplitude errors by analysis of the same spectrum, and on the other hand to obtain a measure for the time-dependent distribution of the Fe^{3+} ions between the transition aluminas and the α-Al_2O_3.

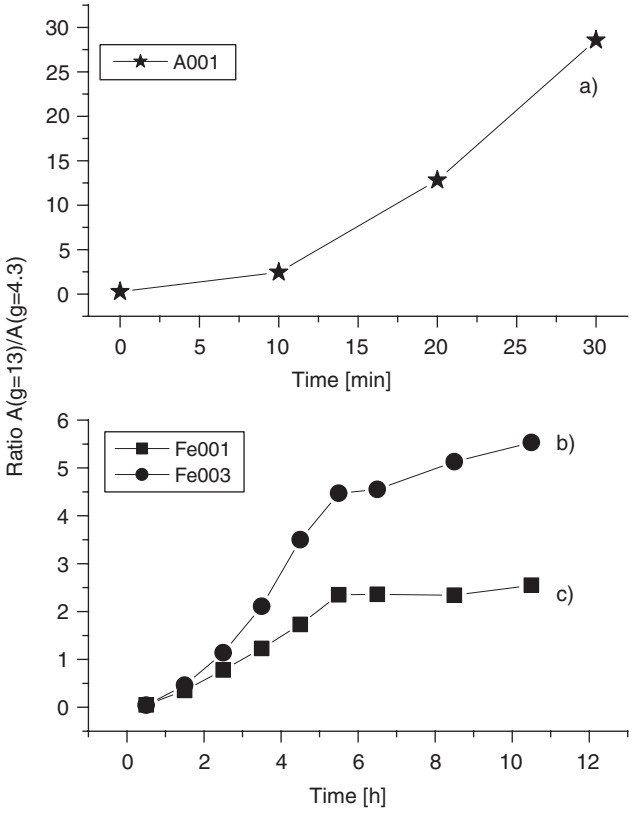

Fig. 9. Time evolution of the ratios of ESR amplitudes of the signals at $g'\sim13$ and 4.3 for (a) the nominally undoped sample A2 after heat treatments (performed in ESR tubes) at 1150 °C for different time periods and (b, c) samples of different doping levels after heat treatments (performed in ESR tubes) at 750 °C.

With small Fe^{3+} concentrations (e.g. in the nominally undoped samples) and after a short induction period at $T = 1150$ °C, the Fe^{3+} signals in α-Al_2O_3 ($g'\sim13$) dominate at the expense of the intensity of resonance with $g'\sim4.3$ (Fig. 9a).

The samples doped with Fe^{3+} behave in quite a different manner; local α-Al_2O_3:Fe^{3+} formation (Fig. 9b and c) can be observed even at 750 °C here (e.g. look at the signal in Fig. 2e, with $g'\sim13$). The induction period is hardly pronounced and after 5 h there is a quotient rise, with a transition to quasi-stationary behaviour. This is an expression of a comparative distribution of Fe^{3+} ions between the α-Al_2O_3 and the transition aluminas under the conditions selected. The higher speed (relative amplitude change per time unit) shown in Fig. 9b for sample Fe003 corresponds to the higher Fe^{3+} concentration (see Table 1). The quasi-stationary state is reached, when all accessible and suitable Fe_2O_3 species are being used as seeds and consequently only a small concentration of Fe^{3+} is embedded in the corundum at this temperature (750 °C).

Fig. 10 makes clear the changes which take place in the samples in an oxygen or hydrogen atmosphere (at 1000 °C) and which are sensitively indicated by Fe^{3+}-ESR spectra. A significant number of species with $g'\sim4.3$ remains after tempering in hydrogen (1 h, 1000 °C), both in the cases of sample Fe026 as well as of S200 (likewise with a small Fe^{3+} concentration on account of impurities), which indicates transition alumina residues. In this connection, it is remarkable that no (local-structural) difference in the two corundum charges could be ascertained from the ^{27}Al-MAS-NMR perspective after tempering in oxygen or hydrogen [36]. As oxygen favours the formation or structural perfecting of corundum, it should also contribute to the complete in situ transformation of Fe^{3+} species or of the entire matrix into α-Al_2O_3:Fe^{3+} at $p_{O_2}\sim1$ bar.

Finally, attention is drawn to an interesting comparison here: TA in nitrogen atmosphere produced no crystallisation peak T_p for the seeded sample S200 after pre-treatment in hydrogen at 1000 °C; i.e. even after reduction, typical seed behaviour continued and the sample was transformed at just 1000 °C (evidenced by X-ray diffraction). With sample Fe026, a crystallisation peak was shown to exist after the same pre-treatment, the value of which fitted well into the graph (Fig. 1a). That is, residues of small Fe_2O_3 aggregates were present in the sample as a result of incomplete reduction.

The seeded sample S200 treated in oxygen for 1 h at 1000 °C provides a relatively intensive signal of α-Al_2O_3/Fe^{3+}, i.e. the Fe^{3+} that is present as contamination is with the support of oxygen completely incorporated in the corundum.

At $g'\sim13$, the relatively small signal that was obtained for sample S200 treated in hydrogen is evidence of slight Fe^{3+} incorporation and implicitly indicates a substantial

Fig. 10. ESR spectra of the samples Fe026 and S200 after heat treatments at 1000 °C for 1 h (quartz tubes with 2 cm inner diameter) in oxygen and hydrogen atmospheres, respectively: (a) sample Fe026, oxygen, (b) sample Fe026, hydrogen, (c) sample S200, oxygen and (d) sample S200, hydrogen. The intensities at $g'\sim13$ of the spectra (b) and (d) are equal to 1/7 and 1/70 of those of the spectra (a) and (c), respectively.

reduction of existing Fe^{3+} and Fe^{2+} ions, without explicitly observing the magnetically ordered species, as in Fig. 2c. Clearly, the α-Al_2O_3 grows on the surface of the seeds even after hydrogen treatment, in parallel with the reduction reaction.

3.2.4. ESR X-band spectra of milled xerogels as well as milled mixtures of xerogels with selected solid Fe^{3+} compounds before and after thermal analysis

For these experiments a xerogel with a very low iron level (sample A3) was used. Differing from sample A1 it initially showed no resonance in the ESR spectra.

After milling, the nominally undoped xerogels provide new ESR intensities, which are very slight and which are largely settled within the range $g'\sim4.3$. After TA in a nitrogen atmosphere, the typical Fe^{3+} in corundum signals can be recorded (see also Fig. 2a).

Next, the phase Fe_2O_3 was studied. The ESR spectrum consisting of a broad line at $g'\sim2$ shows a clear but yet unspecific influence of the milling process, such as must be expected in spin-exchange coupled systems. Subsequently, after performing milling together with the already activated xerogel, the ESR provides an enhanced signal intensity, with $g'\sim4.3$; i.e. more or less discrete, magnetically uncoupled centres come into being.

TA provides a T_p value of 987 °C for this system that is lower than that of a mechanically activated xerogel ($T_p = 1009$ °C).

If the TA is interrupted even at 850 °C, the ESR provides a clearly increased intensity with $g'\sim4.3$, as well as with $g'\sim2$. There have so far been no indications as to local corundum formation under the selected conditions. On interrupting the TA at 982 °C (i.e. at the steepest slope of the transition peak), an ESR spectrum was obtained which is dominated by typical resonances of Fe^{3+} incorporated in corundum (α-Al_2O_3:Fe^{3+}). But the peaks at $g'\sim13$; 5.2 and 2, are comparably broad owing to the large Fe^{3+} presence by virtue of magnetic dipole–dipole interactions. Furthermore, the co-existence of the transition aluminas and the α-Al_2O_3 phase has been recorded on account of the typical g' values ($g'\sim4.3$ and 13). The corresponding integrals make the existence of Fe_2O_3 regions probable on account of the very broad transition with $g'\sim2$.

Magnetite (Fe_3O_4) was included into the mechanical activation process with regard to a possible effect of low-valent Fe species. Milling of a xerogel containing only small traces of Fe^{3+} (A3) together with 1 wt% Fe_3O_4 yields broad ESR lines which are in principle comparable with those of milled magnetite.

After the TA of the sample has been completed in a nitrogen atmosphere the ESR pattern for α-Al_2O_3:Fe^{3+} is produced, whereby the transition with $g'\sim5.3$ (see also [29,31,37]) is comparatively broad. A T_p of 1008 °C results.

The same value for T_p is achieved with a sample with a Fe_2O_3 addition of 1 wt% (A3Fe_2O_3M) whereby local oxidic species such as distorted Fe_3O_4 and possibly also Fe^0 arise through the reducing conditions (10% H_2/90% N_2 gas atmosphere) of the TA.

The greatest effect regarding the T_p is achieved on milling the xerogel A3 with Fe_2O_3. Here the T_p, at 987 °C, lies distinctly below the value for the mechanically activated xerogel matrix, in which $T_p = 1128$ °C. The largest ESR intensity after performing TA was achieved in this series with the addition of $Fe(acac)_3$, as here the T_p value is at its highest. With a $T_p = 1038$ °C ($\Delta T = -8\%$), the T_p value of the mechanically activated matrix is just about reached.

The finding that the milled sample A3Fe_2O_3M yields a distinct lowering of T_p serves as a further example for the assumption derived from macroscopic findings that the Fe^{3+} ions take effect on T_p in the oxidic form (e.g. Fe_2O_3), and not through some other bonded or complex structure.

4. Discussion

4.1. New findings of thermal analysis

The following can be determined from the experiments that have been carried out: Coupled dehydration/hydration processes occur as a function of the partial water-vapour

pressure p_{H_2O}, whereby the T_p can be significantly decreased. The T_p values that were originally lowered by means of Fe^{3+} doping are raised to distinctly higher values with the use of reducing conditions during TA. The pre-treatment under hydrogen of the xerogel samples (which contain Fe^{3+}) within a temperature range of 300–1000 °C likewise manifests itself by raising the T_p to higher values, which leads to the conclusion that the Fe^{3+} species can take effect at even lower temperatures. Different processes have to be taken into account: Obviously, the reduction of Fe^{3+} species appears to be the main effect at the increase of T_p. It holds also for nominally undoped samples containing traces of Fe^{3+}. In addition to this process, especially effective at higher temperatures of pre-treatment, parallel to the reduction of Mn^{3+} and Mn^{4+} species, a deactivation at the surface of the matrix particles should be considered. This e.g. concerns surface seeds, formed spontaneously by the matrix and phenomenologically observed by the H_2 influence on samples containing only traces of iron (see for example the boehmite samples in Fig. 1).

The xerogels [2,16], which contain nitrates, within the temperature range from ~200 to ~350 °C, produce during the course of the TA in a 10% hydrogen/90% nitrogen atmosphere a multitude of exothermic peaks, which are unexpectedly sharp (not shown here). A trapping of NO_2 as described in [2] before has not been observed under reducing conditions.

All in all, the maximum temperature belonging to the transformation peak T_p has proved to be a function of numerous influences, important ones are:

- the concentration of Fe^{3+} ions that are not bound up with complexing ligands (e.g. acetylacetonate groups); Fe^{3+} ions are active in small Fe_2O_3 clusters, phase precursors or active $\{Fe^{3+}–O_x\}$ particles;
- the possible stabilisation of the precursors of the γ-Al_2O_3 phase by Fe^{3+} ions, whereby this effect significantly loses its potency to phase separation (the formation of an $\{Fe–O_x\}$ phase that is ineffective in seed formation) above concentrations of about 0.2 mol% Fe_2O_3;
- pre-tempering in a temperature range of 150–300 °C; here a structural reorganisation and an activation of Fe^{3+}-doped xerogels take place with simultaneous enlargement of ESR amplitudes, with g'~4.3;
- the activation state of the xerogel matrix, i.e. the degree of amorphisation, particularly the state after mechanical activation, whereby the activation barrier for the transition of xerogel to γ-Al_2O_3 is lowered;
- the TA heating rate, as both thermodynamic and kinetic effects determine the position and width of the transition peak to α-Al_2O_3;
- the seeds that are formed internally as well as those already added to the sol [2,5];
- the atmosphere in which thermal energy is supplied, particularly p_{O_2}, p_{H_2}, p_{H_2O} whereby the effect of these three atmospheres may be completely different;
- the synthesis route of xerogels (sequence and manner of educt admixture, temperature–time regime, among others).

4.2. Information obtained by Fe^{3+}-ESR with respect to spectroscopic and material aspects

The habit for X-band spectra of Fe^{3+} ions is determined by the following species in the investigated samples: Together with small $\{Fe–O_x\}$ aggregates, the Fe^{3+} ions (e.g. as Fe^{3+}_{aq}) in the sol or xerogel matrix produce spectra of the type shown in Fig. 2d, with a resonance of narrow width with g'~4.3 and a broad width with g'~2 (proven by the respective integrals); the corresponding intensity relationships represent the distribution of Fe^{3+} ions between the co-existing phases and precursors, respectively.

As soon as the corundum matrix has formed as such (even locally, if need be), it constrains the trigonal symmetry [29,37] of the FeO_6 co-ordination for the initially incorporated or finally diffused Fe^{3+} ions yielding the typical X-band pattern of the Fe^{3+} fine structure (see also Fig. 2a).

Further discrete spectral phenomena occurred only in the interim and indicate Fe^{3+} species with an oxygen co-ordination in the transition region between orthorhombic and trigonal symmetry.

After simulation [29,31] and comparison of experimental and simulated spectra, the X-band spectra of the untreated, pre-treated or thermally analysed samples facilitate access to the following information: It has to be assumed that at least three or four phases co-exist up to the temperature T_p.

The largest available Fe^{3+} amounts are embedded in the corundum matrix that is coming into being in an oxygen atmosphere at sufficiently high temperatures ($T \geqslant 1000$ °C) up to concentrations of Fe^{3+}~0.1 mol%. Thereby, the Fe^{3+} ions increasingly lose their proven indicator function regarding the quantity and quality of the corundum formed, with tiny Fe^{3+} concentrations.

The effectiveness with which Fe^{3+} ions are embedded in the corundum matrix and also the degree of local structural organisation increase with rising temperature of transformation to α-Al_2O_3. Thereby, the diffusion of Fe^{3+} in the still existing transition aluminas with subsequent (coupled) transformation into doped corundum (α-Al_2O_3:Fe^{3+}) is being given greater importance in contrast to the direct diffusion of Fe^{3+} in native corundum. At the same time, the competition that has become apparent (particularly at low temperatures) between phase separation into α-Al_2O_3 and Fe_2O_3 could be checked.

The formation of α-Al_2O_3:Fe^{3+} can be ESR spectroscopically proven with the increase in (local) partial water-vapour pressure even at T~750 °C. Coupled hydration/dehydration processes obviously contribute to the formation of colonies of the phase being constituted.

The spin exchange interaction, which serves here as an important indicator for the aggregation of paramagnetic

species, can be evidenced by line shape analysis of individual signals within the range $g' \sim 2$ (see Fig. 2c).

Determination of the proportion of α-Al_2O_3:Fe^{3+} as well as transition aluminas sensitively arises from the amplitude ratio with $g' \sim 13$ and 4.3 (or from the respective integrals).

Conclusions about the aggregation of Fe^{3+} and Fe^{2+} ions in the formation of $\{Fe^{2+}–O–Fe^{3+}\}$ species as well as the development of magnetic order phenomena in the samples result from the temperature dependence of the spectral transitions; as expected, species arise under reducing conditions with a ferri-/ferromagnetic coupling in an analogous manner to disturbed magnetite and its ESR spectroscopic behaviour. If the particles are sufficiently small, this phenomenon appears as super-paramagnetism.

The following consideration may be helpful when describing the formation of aggregated $\{Fe^{3+}–O_x\}$ species: Without pre-treatment, the xerogels provide small signals that are not further differentiated with respect to the level of doping, at $g' \sim 4.3$. Clearly, the greater proportion of the existing Fe^{3+} ions contribute to a very broad signal in each case, with $g' \sim 2$. The brown colouration of the more highly doped samples corresponds to other Fe^{3+} organic compounds, or to aggregation process products of the $\{Fe^{3+}–O_x\}$ species. The ESR intensity at $g' \sim 4.3$ increases strongly after tempering at 300 °C (with and without a hydrogen atmosphere). The cause of this may be the thermally simulated incorporation of Fe^{3+} in the AlOOH phase that is evolving, accompanied by dehydration and aggregation processes.

4.3. Chemical and physical consequences of thermally and mechanically induced redox processes

Oxidation–reduction processes in xerogels have a number of causes: the oxidative effect of decomposing nitrate residues, the reductive effect of decomposing organic residues, as well as the externally predetermined atmosphere (p_{O_2}, p_{H_2}, p_{H_2O}) [16,38,39]. The use of external reductive conditions (a hydrogen atmosphere within a temperature range of 300–1000 °C, TA in a reducing gas atmosphere) brings about a reduction of the Mn^{x+} species ($x = 3$ or 4) formed as an intermediate in the lower temperature range (up to about 500 °C), or of appropriate aggregates to Mn^{2+}. In contrast to this, Fe^{3+} amounts have exhibited relatively few changes, which makes one conclude that discrete co-ordination is at work. Above 500 °C the doped matrices were reductively changed, with T_p increases as a result. Moreover, it became apparent which $\{Fe–O_x\}$ species can be reduced under the applied conditions. This largely concerns aggregated $\{Fe–O_x\}$ species, and hardly Fe^{3+} point defects in discrete phases (see below). This gave rise to the further point that the effective components for lowering the T_p are provided by small active particles of Fe_2O_3, resulting from the Fe^{3+} doping of sols (see also [3,4]).

Altogether, the thermal pre-treatment of samples under hydrogen led in any case to higher T_p values, whereby the respective shifts were in part slight. The effect is most strongly pronounced with comparatively small Fe^{3+} concentrations at 850 °C. Clearly, the positive re-organisation effect of the matrix was dominant in the lower temperature range in comparison with the decreasing reductive effect of hydrogen.

At higher Fe^{3+} concentrations the reduction factor asserts itself as a result of phase separation (the co-existence of transition aluminas and Fe_2O_3); during its further course, an iron pool of Fe species with different valences forms at the beginning of phase separation and engages in the reaction and transformation of Fe^{3+}-doped α-Al_2O_3.

T_p shifts to distinctly higher values result when carrying out the TA of Fe^{3+}-doped samples under reducing conditions; i.e. the values for undoped samples are nearly reached. Another consequence of this is that the small and reducible $\{Fe–O_x\}$ aggregates (indicated by very broad signals with $g \sim 2$ and by broadened transitions in the case of $g' \sim 4.3$), are to be regarded as effective components for the T_p shift. In contrast with this, the corundum seeded samples show very little influence of the reductive atmosphere on T_p; however, the intensity relationships of the ESR signals for slight Fe^{3+} impurity concentrations are changed with $g' \sim 13$ and 4.3 (Fig. 8a). They reflect the distribution of Fe^{3+} ions between the transition aluminas and α-Al_2O_3.

Obviously, α-Al_2O_3 can scarcely grow on the $\{Fe^{2+}–O–Fe^{3+}\}$ species (see Fig. 2b and c and the experiments on the milled sample A3Fe_3O_4M) formed by reduction (see also [2]). As corundum formation nevertheless takes place in the samples during TA, it may be assumed that this occurs spontaneously and on the other hand that in the presence of suitable, smaller Fe_2O_3 particles at least two sub-systems must be present in the unreduced samples with finite Fe^{3+} concentrations.

The strongly disturbed magnetite precursors ("Fe_3O_4" or mixed valence cluster of the type $\{Fe^{2+}–O–Fe^{3+}\}$ (Fig. 2b and c) arise in a reducing atmosphere at higher temperatures. These spectroscopically reflect the combined effect of aggregation and magnetic order, which depends on local and naturally also on the original Fe^{3+} concentration of the xerogels. Together with the finding that Fe^{3+} ions, localised on α-Al_2O_3 lattice sites, or in transition aluminas, cannot be, or can hardly be, reduced under the prevailing conditions, also at this point it may be concluded that small, reducible Fe_2O_3 particles are the effective components for the shift of the transformation peak.

The use of mechanical energy in the milling process not only causes an activation of the xerogel matrix, accompanied by defect formation and the release of water. It also leads to the first stages of solid-state reaction between the matrix and the jointly milled Fe_2O_3. Thus magnetically non-collective, ortho-rhombically distorted

{Fe–O_x}-species come into being with a resonance of $g'\sim4.3$. These species are caused by a thermally induced diffusion of Fe^{3+} ions into the xerogel matrix as well as of Al^{3+} ions into the Fe_2O_3 matrix. To summarise: a currently indefinable perturbation occurs in the spin exchange (e.g. as a result of very slight changes to the bonding angle) in the Fe–O systems as a result of the use of mechanical–thermal energy, which is spectroscopically indicated by a line form change. Indeed, milled Fe_2O_3 provides a very broad ESR signal that can hardly be further evaluated and does not permit the specifying of defects. But the evidence of the effect of small Fe_2O_3 particles on the lowering of T_p is a sure thing. This statement is supported by further milling findings concerning the admixture of Fe_3O_4, $Fe(acac)_3$, etc., which document that active Fe_2O_3 particles are clearly required for the T_p shift. Any disturbance by the interactions with other valence stages of iron or by the residues of complex formers is of disadvantage. Favoured by the activated and geometrically suitable, small Fe_2O_3 particles (fulfilling the requirement of surface coherence) α-Al_2O_3 can grow and incorporate amounts of Fe^{3+} in dependence on the transformation temperature. In addition to the diffusion of Fe^{3+} ions into the freshly formed corundum, precursors with resonances at $g'\sim4.3$ are mainly to be formed which finally convert to the doped system α-Al_2O_3:Fe^{3+} ($g'\sim13$; 5.2; Fig. 2a). Consequently, even under these conditions there is a distribution of Fe^{3+} ions between different phases (transition aluminas, corundum, Fe_2O_3, {Fe–O_x}. This becomes particularly apparent when using samples in which the TA was interrupted at 850 or 982 °C.

If one compares the effects observed with the milled xerogels and the redispersable boehmites, then it is apparent that the highest T_p value (1220 °C) was determined for the latter. Both systems possess very low Fe^{3+} concentrations and matrix particles of small size. In contrast to the milled xerogels which supply a large number of crystallisation seeds and which consequently accelerate the transformation process, the redispersable boehmites are crystalline and their surfaces are conditioned for re-dispersion; hence precisely the aggregation necessary for the phase transformation is prevented.

5. Conclusions

The effective components for the lowering of T_p are clearly small {Fe–O_x} aggregates (Fe_2O_3) which for the growth of α-Al_2O_3:Fe^{3+} are characterised by sufficient activity and surface coherence. By way of contrast, non-aggregated or little-aggregated Fe^{3+} species largely have a role as indicators for recognising the advance of thermal or mechanically induced processes as well as for the characterisation of non-crystalline components or developing phase precursors. As soon as the corundum matrix has formed as such (even locally, if need be), it constrains the FeO_6 polyhedrons of the initially incorporated or finally diffused Fe^{3+} ions into trigonal asymmetry [29,37]. As a result the typical X-band pattern for the fine structure is observed (see also Fig. 2a).

Based on the findings of ESR, TA, and XRD it has to be assumed that at least three or four phases co-exist up to the temperature T_p. The Fe^{3+} ions distribute themselves between these phases as a function of the available Fe^{3+} concentration, the tempering period and temperature, the atmosphere and the possible presence of chelating agents.

The proportion of small aggregates increases with the Fe^{3+} concentration; phase transformation and the structural perfecting of the matrix are accomplished in parallel with cluster formation under the combined effect of thermal energy and increasing reduction power; with the samples Fe013 and Fe052, the {Fe^{3+}–O_x} species still exerts a distinct influence on the transition temperature T_p.

The small {Fe–O_x} aggregates disclose the following to ESR spectroscopy: In addition to the characteristic line widths and shapes (particularly with the exchange-coupled species), distinct deviations of ESR intensities from the Curie Law occur when varying the measuring temperature (see also [32]).

A further important indication is not only the chemical reducibility, but also the shift of T_p to lower values.

Acknowledgments

Dr. A. Zehl is kindly acknowledged for support at carrying out the ESR measurements. The Deutsche Forschungsgemeinschaft (DFG) is acknowledged for financial support (STO 301/2-3, PO405/6-1).

References

[1] L.A. Xue, I.-W. Chen, J. Mater. Sci. Lett. 11 (1992) 443–445.
[2] M. Nofz, R. Stösser, G. Scholz, I. Dörfel, D. Schultze, J. Eur. Ceram. Soc. 25 (2005) 1095–1107.
[3] J.L. McArdle, G.L. Messing, Adv. Ceram. Mater. 3 (1988) 387–392.
[4] J.L. McArdle, G.L. Messing, J. Am. Ceram. Soc. 76 (1993) 214–222.
[5] R. Stößer, G. Scholz, J.-Y. Buzaré, G. Silly, M. Nofz, D. Schultze, J. Am. Ceram. Soc. 88 (2005) 2913–2922.
[6] P. Souza Santos, H. Souza Santos, S.P. Toledo, Mater. Res. 3 (2000) 104–114.
[7] C. Wolverton, K.C. Hass, Phys. Rev. B 63 (2000) 024102-1–024102-16.
[8] M. Digne, P. Sautet, P. Raybaud, H. Toulhoat, E. Artacho, J. Phys. Chem. B 106 (2002) 5155–5162.
[9] M. Digne, P. Sautet, P. Raybaud, P. Euzen, H. Toulhoat, J. Catal. 211 (2002) 1–5.
[10] A. Braun, M. Wolff, R. Clasen, S. Schlabach, Bin. Xu, D. Vollath, Ceram. Eng. Sci. Process. 24 (2003) 115–120.
[11] Y.-W. Rhee, H.Y. Lee, S.-J.L. Kang, J. Eur. Ceram. Soc. 23 (2003) 1667–1674.
[12] T. Carisey, I. Levin, D.G. Brandon, J. Eur. Ceram. Soc. 15 (1995) 283–289.
[13] F.S. Yen, H.S. Lo, H.L. Wen, R.J. Yang, J. Cryst. Growth 249 (2003) 283–293.
[14] L. Pach, R. Roy, S. Komarneni, J. Mater. Res. 5 (1990) 278–285.
[15] J. Tartaj, G.L. Messing, J. Mater. Sci. Lett. 16 (1997) 168–170.
[16] Y.L. Huang, D.S. Xue, P.H. Zhou, Y. Ma, F.S. Li, Mater. Eng. A 359 (2003) 332–337.

[17] L. Bača, J. Plewa, L. Pach, J. Opfermann, J. Therm. Anal. Calorimetr. 66 (2001) 803–813.
[18] M. del Carmen Prieto, J.M.G. Amores, V. Sanchez Escribano, G. Busca, J. Mater. Chem. 4 (1994) 1123–1130.
[19] P. Tartaj, J. Tartaj, Chem. Mater. 14 (2002) 536–541.
[20] J.A. Weil, J.R. Bolton, J.E. Wertz, Electron Paramagnetic Resonance, Wiley, New York, 1994.
[21] R. Stösser, M. Nofz, Glastech. Ber. Glass Sci. Technol. 67 (1994) 156–170.
[22] R. Stößer, G. Scholz, Report to Deutsche Forschungsgemeinschaft (Germany) Bildung und Einfluss der Gasphase auf die chemische und strukturelle Reorganisation fester Al–F–, Al–(O, F)– und Al–O– Verbindungen (Formation and influence of the gas phase on the chemical and structural reorganisation of solid Al–F–, Al–(O, F)– and Al–O– compounds), Berlin, 2000, STO301/2-2, 2-3
[23] R. Stößer, M. Nofz, W. Geßner, Ch. Schröter, G. Kranz, J. Solid State Chem. 81 (1989) 152–164.
[24] W.-D. Emmerich, E. Post, J. Therm. Anal. 49 (1997) 1007–1012.
[25] E. Kaisersberger, E. Post, Thermochim. Acta 295 (1997) 73–93.
[26] B.R. Angel, W.E.J. Vincent, Clays Clay Miner. 26 (1978) 263–272.
[27] A.J. Herbillon, M.M. Mestdagh, L. Vielvoye, E.G. Derouane, Clay Miner. 11 (1976) 201–220.
[28] R. Berger, J. Kliava, E.-M. Yahiaoui, J.-C. Bissey, P.K. Zinsou, P. Béziade, J. Non-Cryst. Solids 180 (1995) 151–163.
[29] G. Scholz, R. Stösser, M. Krossner, J. Klein, Appl. Magn. Res. 21 (2001) 105–123.
[30] G. Scholz, R. Stößer, T. Grande, S. Aasland, Ber. Bunsengesellschaft Phys. Chem. 101 (1997) 1291–1296.
[31] J.-Y. Buzaré, G. Silly, J. Klein, G. Scholz, R. Stösser, M. Nofz, J. Phys.: Condens. Matter 14 (2002) 10331–10348.
[32] R. Stößer, R. Brenneis, M. Nofz, N. Steinfeld, J. Mater. Sci. 31 (1996) 1405–1413.
[33] W.E. Blumberg, in: A. Ehrenberg, B.E. Malström, T. Vänngärt (Eds.), Magnetic Resonance in Biological Systems, London, Pergamon Press, 1967, p. 111.
[34] R. Stößer, G. Scholz, Appl. Magn. Res. 12 (1997) 167–181.
[35] D. Tchoubar, J.-Y. Bottero, C.R. Acad. Sci. Paris 322 (IIa) (1996) 523–534.
[36] J.-Y.- Buzaré, private communication.
[37] R.S. de Biasi, D.C.S. Rodrigues, J. Am. Ceram. Soc. 68 (1985) 409–412.
[38] Z. Hrabě, O.M. Spaldon, L. Pach, J. Kozánková, Mater. Res. Bull. 27 (1992) 397–404.
[39] K. Sohlberg, S.J. Pennycook, S.T. Pantelides, J. Am. Chem. Soc. 121 (1999) 7493–7499.